

# Nuclear deformation as a source of the non-linearity of King plot in the Yb<sup>+</sup> ion.

Saleh O. Allehabi, V. A. Dzuba, and V. V. Flambaum

*School of Physics, University of New South Wales, Sydney 2052, Australia*

A. V. Afanasjev

*Department of Physics and Astronomy, Mississippi State University, Mississippi 39762, USA*

(Dated: December 9, 2020)

We perform atomic relativistic many-body calculations of the field isotope shifts and calculations of corresponding nuclear parameters for all stable even-even isotopes of Yb<sup>+</sup> ion. We demonstrate that if we take nuclear parameters of the Yb isotopes from a range of the state-the-art nuclear models which all predict strong quadrupole nuclear deformation, then calculated non-linearity of the King plot, caused by the difference in the deformation in different isotopes, is consistent with the non-linearity observed in the experiment (Ian Counts *et al*, Phys. Rev. Lett. **125**, 123002 (2020)). The changes of nuclear RMS radius between isotopes extracted from experiment are consistent with those obtained in the nuclear calculations.

In recent paper [1] the non-linearity of the King plot has been observed. The authors state that the effect may indicate physics beyond the Standard Model (SM), or, within the SM, may come from the quadratic field shift (QFS). Possible non-linearity of the King plot in Yb<sup>+</sup> was studied theoretically in Ref. [2]. In the present paper we show that it is more likely that the observed non-linearity of the King plot is due to a significant non-monotonic variation of the nuclear deformation in the chain of isotopes. We perform nuclear and atomic calculations of the field isotope shift (FIS) which include nuclear deformation and demonstrate that the dependence of the deformation on isotopes leads to a non-linearity of the King plot which is consistent with the observations in Ref. [1]. We show that the comparison of theoretical and experimental non-linearities can be used to discriminate between different nuclear models, favoring some and disfavoring others.

It is well known from experimental nuclear rotational spectra [3] and its theoretical interpretation [4, 5] as well as from presented below nuclear calculations that all even-even Yb isotopes studied in [1] have deformed nuclear ground states with the parameters of the quadrupole deformation  $\beta \sim 0.3$ . In our previous paper [6] we demonstrated that nuclear deformation may lead to a non-linearity of the King plot.

Therefore, in the present paper we calculate FIS in even-even Yb isotopes with accounting of nuclear deformation. We treat Yb<sup>+</sup> as a system with one external electron above closed shells and use the correlation potential method [7]. We calculate the correlation potential  $\hat{\Sigma}$  in the second order of the many-body perturbation theory. Correlation potential is the non-local (integration) operator responsible for the correlation corrections due to interaction between valence electron and electrons in the core. Then we use  $\hat{\Sigma}$  to calculate the states of valence electron (numerated by  $v$ ) in the form of the Brueckner

orbitals (BO)

$$(\hat{H}^{\text{HF}} + \hat{\Sigma} - \epsilon_v)\psi_v^{\text{BO}} = 0. \quad (1)$$

Here  $\hat{H}^{\text{HF}}$  is the relativistic Hartree-Fock (HF) Hamiltonian for the closed-shell core of Yb<sup>+</sup>,

$$\hat{H}^{\text{HF}} = c\hat{\alpha}_i \cdot \hat{p}_i + (\beta - 1)mc^2 + V_{\text{nuc}}(r_i) + V_{\text{core}}(r_i). \quad (2)$$

In this expression  $\alpha$  and  $\beta$  are the Dirac matrices,  $V_{\text{nuc}}$  is nuclear potential obtained by integrating nuclear charge density,  $V_{\text{core}}$  is the self-consistent HF potential and the index  $i$  numerates single-electron states.

FIS is calculated by varying nuclear potential  $V_{\text{nuc}}$  in (2). The RPA+BO method is similar to the MBPT (Many Body Perturbation Theory) method used in [1]. The results are presented in the form (see also [1]), in which index  $a$  numerates atomic transitions,

$$\nu_a^{\text{FIS}} = F_a \delta \langle r^2 \rangle + G_a^{(2)} \delta \langle r^2 \rangle^2 + G_a^{(4)} \delta \langle r^4 \rangle. \quad (3)$$

First term in this equation is the standard FIS, other two terms are corrections responsible for the non-linearity of the King plot. The term with  $G_a^{(2)}$  is due to the second order effect in the change of the nuclear Coulomb potential called the quadratic field shift (QFS) and the last term appears mainly due to the relativistic effects in the electron wave function, i.e. these terms represent different physical phenomena. On the other hand, their effects on the isotope shift are similar. It was suggested in Ref. [1] that  $\langle r^4 \rangle$  and  $\langle r^2 \rangle$  are related by  $\langle r^4 \rangle = b \langle r^2 \rangle^2$ , where  $b$  is just a numerical constant,  $b = 1.32$ . Extra care should be taken in calculating  $G^{(2)}$  and  $G^{(4)}$  independently on each other. For example, they cannot be defined simultaneously in a fitting procedure. Therefore, we start the calculations by eliminating the QFS term, i.e. by considering FIS in the linear approximation. The change of the nuclear Coulomb potential between two isotopes is considered as a perturbation and is treated in the first order using the random phase approximation

(RPA). The RPA equations for core electrons have the following form [7]:

$$(\hat{H}^{\text{HF}} - \epsilon_c)\delta\psi_c = -(\delta V_N + \delta V_{\text{core}})\psi_c, \quad (4)$$

where  $\delta V_N$  is the difference between nuclear potentials for the two isotopes, index  $c$  numerates states in the core,  $\delta V_{\text{core}}$  is the change of the self-consistent HF potential induced by  $\delta V_N$  and the changes to all core functions  $\delta\psi_c$ . The equations (4) are solved self-consistently for all states in the core with the aim of finding  $\delta V_{\text{core}}$ . The FIS for a valence state  $v$  is then given by

$$\nu_v^{\text{FIS}} = \langle \psi_v^{\text{BO}} | \delta V_N + \delta V_{\text{core}} | \psi_v^{\text{BO}} \rangle. \quad (5)$$

Apart from eliminating the QFS, an important advantage of using the RPA method (where the small parameter, i.e. the change of the nuclear radius, is explicitly separated) is the suppression of a numerical noise. Non-linearity of the King plot is extremely small and direct full scale calculations of the change of the atomic electron energy due to a tiny change of the nuclear radius (i.e. without the separation of the small parameter) may lead to a false effect in the King plot non-linearity (see below). After FIS is calculated for a range of nuclear parameters, the constants  $F_a$  and  $G_a^{(4)}$  are found by fitting the results of the atomic calculations by formula (3) (without  $G^{(2)}$ ) by the least-square-root method.

To calculate  $G^{(2)}$  we use the second-order perturbation theory

$$G_a^{(2)} = \sum_n \frac{\langle a | \delta V_N + \delta V_{\text{core}} | n \rangle^2}{E_a - E_n} / \delta \langle r^2 \rangle^2. \quad (6)$$

Here  $\delta V_N$  is the change of nuclear potential between two isotopes. Summation goes over complete set of the single-electron basis states, including states in the core and negative-energy states. To include the core-valence correlations one can use BO for single-electron states  $a$  and  $n$ . Again, the perturbation theory is used instead of the direct calculation of the change of the electron energy due to the tiny change of the nuclear radius to suppress numerical noise.

Instead of the direct summation over electron states in Eq. (6) one can first solve the RPA equation for the valence state  $a$

$$(\hat{H}^{\text{HF}} + \hat{\Sigma} - \epsilon_a)\delta\psi_a^{\text{BO}} = -(\delta V_N + \delta V_{\text{core}})\psi_a^{\text{BO}}, \quad (7)$$

and then use

$$G_a^{(2)} = \langle \delta\psi_a^{\text{BO}} | \delta V_N + \delta V_{\text{core}} | \psi_a^{\text{BO}} \rangle / \delta \langle r^2 \rangle^2. \quad (8)$$

We obtain the same results using Eqs. (6) and (8). This provides a test of the numerical accuracy.

*a. Nuclear deformation.* The quadrupole nuclear deformation  $\beta$  provides a measure of the deviation of the nuclear density distribution from spherical shape so that nuclear radius  $r_n(\theta)$  in the  $\theta$  direction with respect of the

TABLE I: Calculated parameters of formula (3) for the FIS in two transitions of  $\text{Yb}^+$ ;  $a$  stands for the  $6s_{1/2} - 5d_{5/2}$  transition and  $b$  stands for the  $6s_{1/2} - 5d_{3/2}$  transition. Case 1 corresponds to deformed nuclei, while case 2 corresponds to spherical nuclei.

Case	Transition	$F$	$G^{(2)}$	$G^{(4)}$
		GHz/fm <sup>2</sup>	GHz/fm <sup>4</sup>	GHz/fm <sup>4</sup>
1	$a$	-17.6035	0.02853	0.01308
	$b$	-18.0028	0.02853	0.01337
2	$a$	-18.3026	0.02853	0.01245
	$b$	-18.7201	0.02853	0.01273

axis of symmetry is written as  $r_n(\theta) = r_0(1 + \beta Y_{20}(\theta))$ . Electron feels nuclear density averaged over the nuclear rotation (see e.g. Ref. [6]). We calculate the average density by integrating the deformed density over  $\theta$ .

To determine the values of  $F$  and  $G^{(4)}$  parameters in Eq. (3), we first vary the nuclear root-mean-square (RMS) charge radius  $r_c$  and the quadrupole deformation parameter  $\beta$  in the range determined by the nuclear theory (see below):  $5.234 \text{ fm} \leq r_c \leq 5.344 \text{ fm}$  and  $0.305 \leq \beta \leq 0.345$ , and then fit the  $F$  and  $G^{(4)}$  parameters by the formula (see also [6, 8])

$$\nu^{\text{FIS}} = F\delta\langle r^2 \rangle + G^{(4)}\delta\langle r^4 \rangle. \quad (9)$$

to the results of atomic calculations of FIS for different  $r_c$  and  $\beta$ . The values of  $F$  and  $G^{(4)}$  parameters defined in such a way are presented in Table I. The table also gives the values of the  $G^{(2)}$  parameters calculated using (6) and (8). Note that FIS for the  $d$  states of  $\text{Yb}^+$  is about 2 orders of magnitude smaller than FIS for the  $6s$  states and in QFS small matrix elements for the  $d$  states appears in the second-order while in the calculations of  $F$  in the first order. Therefore, the relative difference in the  $G^{(2)}$  parameters for the  $s - d_{3/2}$  and  $s - d_{5/2}$  transitions is much smaller than the relative difference for the  $F$  parameters.

It was shown in Ref. [1] that  $\langle r^4 \rangle \approx b\langle r^2 \rangle^2$ , where  $b$  is just a numerical constant,  $b=1.32$  [1]. We found that the situation is different in deformed and spherical nuclei. By calculating  $\langle r^4 \rangle$  in both cases we found that the results can be fitted with high accuracy by the formula

$$\langle r^4 \rangle = [b_0 + b_1(r_c^2 - r_0^2) + b_2(\beta - \beta_0)] r_c^2, \quad (10)$$

where  $r_0 = 5.179 \text{ fm}$  and  $\beta_0 = 0.305$ . For deformed nuclei  $b_0 = 1.3129$ ,  $b_1 = -0.0036$ ,  $b_2 = 0.1$ , while for spherical nuclei  $b_0 = 1.2940$ ,  $b_1 = -0.0038$ ,  $b_2 = 0$ .

To study the non-linearity of the King plot we need total isotope shift (including mass shift) for two transitions  $a$  and  $b$ . Then using Eq. (3) one can write for the

TABLE II: Nuclear RMS charge radii ( $r_c$ , fm) and the parameters of quadrupole deformation ( $\beta$ ) of even-even Yb isotopes obtained in different nuclear models. The results obtained in the CDFT are labeled by the names of respective functionals.

$A$	BETA		NL3*		DD-ME2		DD-ME $\delta$		DDPC1		FIT	
	$r_c$	$\beta$	$r_c$	$\beta$	$r_c$	$\beta$	$r_c$	$\beta$	$r_c$	$\beta$	$r_c$	$\beta$
168	5.2950	0.3220	5.28751	0.33186	5.29144	0.33115	5.28820	0.33400	5.29528	0.33790	5.2950	0.3100
170	5.3081	0.3258	5.30500	0.33873	5.31000	0.34028	5.30106	0.33070	5.31318	0.34540	5.3081	0.3184
172	5.3204	0.3302	5.31678	0.33188	5.32056	0.33124	5.31138	0.32024	5.32346	0.33429	5.3204	0.3232
174	5.3300	0.3249	5.32776	0.32203	5.33066	0.32072	5.32356	0.31447	5.33291	0.32152	5.3300	0.3208
176	5.3391	0.3050	5.33868	0.31471	5.34230	0.31436	5.33228	0.30413	5.34420	0.31398	5.3391	0.3156

isotope shift between isotopes  $i$  and  $j$

$$\begin{aligned}
\frac{\nu_{bij}}{\mu_{ij}} &= \frac{F_b}{F_a} \frac{\nu_{aij}}{\mu_{ij}} + \left( K_b - \frac{F_b}{F_a} K_a \right) + \\
&+ \left( G_b^{(2)} - \frac{F_b}{F_a} G_a^{(2)} \right) \frac{\delta \langle r^2 \rangle_{ij}^2}{\mu_{ij}} + \\
&+ \left( G_b^{(4)} - \frac{F_b}{F_a} G_a^{(4)} \right) \frac{\delta \langle r^4 \rangle_{ij}}{\mu_{ij}}.
\end{aligned} \quad (11)$$

Here  $K$  is the electron structure factor for the mass shift,  $\mu = 1/m_i - 1/m_j$  is the inverse mass difference. First line of Eq. (11) corresponds to the standard King plot, second and third lines contain the terms which may cause the King plot non-linearities.

To study these non-linearities we use the least-square fitting of Eq. (11) by the formula  $\nu'_b = A\nu'_a + B$ , where  $\nu' = \nu/\mu$ . The relative non-linearities are calculated as  $\Delta\nu'_b/\nu'_b$ , where  $\Delta\nu'_b$  is the deviation of the isotope shift  $\nu'_b$  from its linear fit. To do the fitting and making King plot we need to know the change of nuclear parameters  $\delta \langle r^2 \rangle$  and  $\Delta\beta$  between the isotopes of interest. We use nuclear calculations for this purpose. Nuclear parameters of the Yb isotopes with even neutron number obtained in different nuclear models are presented in Table II.

In the simplest model, called BETA, the nuclear deformation parameter  $\beta$  in a given nucleus is extracted from measured reduced electric quadrupole transition rate B(E2) for the ground state to  $2^+$  state transition. These values are tabulated in Ref. [18]. We also introduce a hypothetical model (labeled as FIT) which has nuclear parameters leading to very accurate fit of both experimental FIS and the deviations of King plot from linearity. Note that the parameters of the FIT model are not so different from other models, i.e. they are pretty realistic.

The ground state properties of the nuclei under study have also been calculated within the Covariant Density Functional Theory (CDFT) using several state-of-the-art covariant energy density functionals (CEDFs) such as DD-ME2, DD-ME $\delta$ , NL3\* and DD-PC1 [19]. In the CDFT, the nucleus is considered as a system of  $A$  nucleons which interact via the exchange of different mesons and nuclear many-body correlations are taken into account. Above mentioned CEDFs represent three major classes of covariant density functional models which provide accurate description of the ground state properties

(such as deformations, charge radii, etc.) of even-even nuclei across the nuclear chart [19, 20]. The main differences between them lie in the treatment of the interaction range and density dependence. The best global description of experimental data on charge radii has been achieved by the DD-ME2 functional [characterized by RMS deviation of  $\Delta r_{ch}^{rms} = 0.0230$  fm], followed by DD-PC1 [which also provides best global description of binding energies], NL3\* and finally by DD-ME $\delta$  [characterized by RMS deviation of  $\Delta r_{ch}^{rms} = 0.0329$  fm] (see Table VI in Ref. [19] and Fig. 7 in Ref. [20]).

Using the parameters coming from these models we calculate FIS, build the King plot, find its deviations from the linearity and compare the results to the experimental data from Ref. [1]. The results are presented in Table III and Fig. 1. One can see that the values of the experimental and theoretical non-linearities are of the same order of magnitude for all nuclear models. This already means that the nuclear deformation is an important effect which has to be included into the analysis. Moreover, for some models (e.g., BETA, FIT, NL3\*, DDPC1) there is a strong correlation between experimental and theoretical data.

To make sure that the non-linearities come from the nuclear deformation and not from QFS, we perform two tests. In the first test we remove nuclear deformation from the calculations by using the values of  $\langle r^4 \rangle$  in (3) which come from the calculations assuming that all isotopes have spherical shapes. In the second test we put  $b_2 = 0$  in Eq. (10). In both cases the deviations of the King plot from the linearity drop by about an order of magnitude. This means that the nuclear deformation is likely to be the main source of the observed non-linearity of the King plot.

*b. Quadratic field shift.* Ref. [1] argues that QFS is the main source of the non-linearity of the King plot. However, their calculations only provided an upper limit on the non-linearity since the results of CI and MBPT calculations were very different. From our point of view the problem with the calculations in Ref. [1] is that they have not separated a small parameter, the change of the nuclear radius, and obtained FIS from the small difference in the energies of the atomic transitions calculated for different nuclear radii. This is certainly a good approach for the calculation of FIS but it is not good enough to calculate a very small non-linearity which is extremely

TABLE III: The deviations from the linearity of the King plot (in parts of  $10^{-6}$ ). The comparison between experiment [1] and calculations in different nuclear models

Isotope pair	Expt.	BETA	FIT	Nuclear model			
				NL3*	DD-ME2	DD-ME $\delta$	DDPC1
168 - 170	-0.192	0.642	-0.206	-0.037	-0.084	-0.511	-0.080
170 - 172	0.270	-0.607	0.281	-0.159	-0.467	0.546	-0.222
172 - 174	-0.489	-3.05	-0.523	-0.200	-0.028	0.392	-0.198
174 - 176	0.411	3.03	0.448	0.387	0.551	-0.406	0.472

TABLE IV: The deviations from the linearity of the King plot  $\delta$  due to the quadratic field shift. The comparison between experiment [1] and calculations using the  $\delta\langle r^2 \rangle$  values which fit the experimental isotope shift [1]. The deviation  $\delta$  is shown as a function of  $\nu_a/\mu$  (see Eq. (11)).

Isotope pair	Expt.		QFS	
	$\nu_a/\mu$ $10^{11}$ kHz u	$\delta$ $10^{-6}$	$\nu_a/\mu$ $10^{11}$ kHz u	$\delta$ $10^{-6}$
168 - 170	-0.311	-0.192	-0.351	-0.017
170 - 172	-0.299	0.270	-0.337	0.020
172 - 174	-0.236	-0.489	-0.272	0.013
174 - 176	-0.231	0.411	-0.267	-0.016

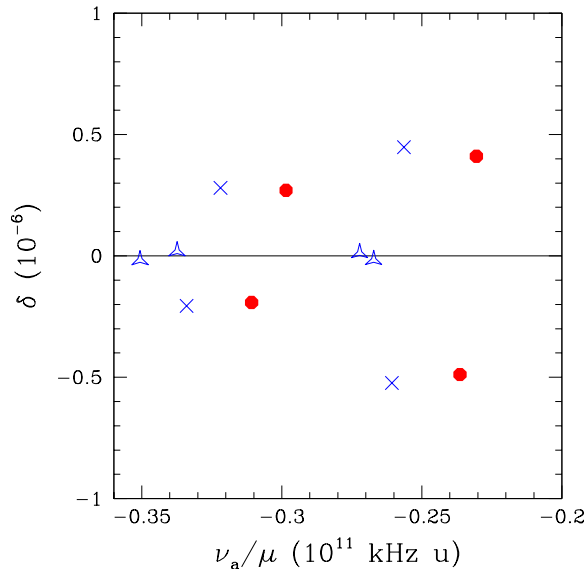


FIG. 1: The deviations from linear King plot in experiment (solid red circles) and theory. Theoretical deviations caused by nuclear deformation are shown as blue crosses, and those by QFS are shown as blue triangles. All theoretical numbers correspond to the FIT nuclear model.

sensitive to numerical noise.

Our results presented earlier indicated that QFS gives a much smaller contribution to the non-linearity of the King plot than the upper limit presented in Ref. [1]. To test this result we performed FIS and QFS calculations by a different method assuming that all isotopes have

spherical nuclear shape ( $\beta = 0$ ). The main motivation for using RPA method in the case of nuclear deformation is the minimization of numerical noise which comes from extra integration over directions. There is no such problem for spherical nuclei and the procedure is less complicated. FIS in this case may be found from the direct variation of the nuclear radius in the nuclear Coulomb potential. We perform HF and BO calculations for a range of nuclear charge RMS radii from  $\langle r^2 \rangle = (5 \text{ fm})^2$  to  $\langle r^2 \rangle = (6 \text{ fm})^2$  and present the results by the same formula (3) (see Table I). As in case of deformed nuclei, the QFS parameter  $G^{(2)}$  is found from the perturbation theory calculations. The values of  $F$  and  $G^{(4)}$  are slightly different.

The same equation (11) and the same procedure were used to find the non-linearities of the King plot. The results are presented on Fig. 1 and Table IV. As one can see, the non-linearity caused by QFS is an order of magnitude smaller than the observations. It is also much smaller than the non-linearity caused by the variation of the nuclear deformation.

We also performed another test calculation using constant value  $\beta = 0.3$  instead of  $\beta = 0$ . Again, without variation of  $\beta$  the non-linearity of the King plot is small.

*c. The change of nuclear RMS charge radius.* Formula (3) with parameters  $F, G^{(2)}, G^{(4)}$  from Table I can be used to find the change of the nuclear RMS charge radius between isotopes by fitting experimental FIS. The values of the  $\delta\langle r^2 \rangle$  corresponding to the best fit (the FIT model in Table II) are presented in Table V and compared with other data. Note that if FIS is calculated using parameters of other nuclear models from Table II then the difference between theory and experiment ranges from few percent to  $\sim 15\%$ . This is because nuclear theory is not sufficiently accurate in predicting  $\delta\langle r^2 \rangle$ . It is easy to see from the data in Table II that 0.01% change in the nuclear RMS radius may lead to  $\sim 10\%$  change in the value of  $\delta\langle r^2 \rangle$  leading to the same change in FIS. Note, however, very good agreement for the  $\delta\langle r^2 \rangle$  between best fit and the predictions of the DD-ME $\delta$  nuclear model (see Tables II and V). This might be fortuitous. This model is not the best in reproducing experimental non-linearities of King plot. We stress that the non-linearities of King plot are more sensitive to the change of nuclear shape rather than to its RMS charge radius.

*d. The comparison with other results for  $\delta\langle r^2 \rangle$ .* It is instructive to analyze possible reasons for the difference

TABLE V: The changes of nuclear RMS charge radius ( $\delta\langle r^2 \rangle$ , fm<sup>2</sup>) extracted from the isotope shift measurements.

Isotope pairs	Ref. [1]		Ref. [12, 13]	This work
	CI	MBPT		
(168,170)	0.156	0.149	0.1561(3)	0.138
(170,172)	0.146	0.140	0.1479(1)	0.130
(172,174)	0.115	0.110	0.1207(1)	0.102
(174,176)	0.110	0.105	0.1159(1)	0.097

between our results and other results for  $\delta\langle r^2 \rangle$  presented in Table V. There is a 12 to 19% difference between our results and those published in Ref. [12] (see Table V). However, the latter were taken from a fifty-years-old paper [13] which has no many-body calculations but only estimations based on the single-electron consideration. The uncertainty of such estimations can be well above 10% and even 20%.

There is also a 8% to 13% difference between our results and those of Ref. [1]. Ref. [1] contains two calculations of the FIS constants performed by CI and MBPT methods with the 4% difference between corresponding results. Our FIS constant  $F$  is about 13% larger than the same constant calculated in Ref. [1] using the CI method and about 8% larger than those calculated in Ref. [1] using the MBPT method. This explains the difference in the results for  $\delta\langle r^2 \rangle$  (Table V). When we use the numbers from Ref. [1] in Eq. (3) we reproduce their results for  $\delta\langle r^2 \rangle$ . The difference in the results seems to be due to the difference in the procedures defining the constants  $F$  and  $G$ . We use BO and the RPA method to calculate  $F$  and  $G^{(4)}$  and the perturbation theory to find  $G^{(2)}$  as it has been explained above. The authors of Ref. [1] calculate  $F$  as a leading term of the Seltzer moment expansion at the origin for the total electron density (see Eq. (S11) in [1]) and then use partial derivatives of FIS to calculate

constants  $G$ . Such method looks sensitive to the degeneracy of  $G^{(2)}$  and  $G^{(4)}$  contributions to FIS. An indication of the problem may be a significant relative difference in  $G^{(2)}$  parameters in Ref. [1] while we argued above that it must be very small since it appears in the second order of the small  $d$  wave FIS matrix elements.

It is instructive to explain why the ratios  $G^{(4)}/F$  are different in the  $s - d_{3/2}$  and  $s - d_{5/2}$  transitions (this is needed for the non-linearity of the King plot without QFS). We suggest the following mechanism supported by the numerical calculations. According to it only two relativistic Dirac wavefunctions,  $s_{1/2}$  and  $p_{1/2}$ , penetrate into the nucleus. They have different spatial distributions inside and therefore the ratios of the  $\delta\langle r^2 \rangle$  and  $\delta\langle r^4 \rangle$  contributions to their energies and wavefunctions are noticeably different. The  $d_{3/2}$  and  $d_{5/2}$  wavefunctions interact differently with the  $s_{1/2}$  and  $p_{1/2}$  ones and this gives the difference in  $G^{(4)}/F$ .

In conclusion we state that presented arguments indicate that nuclear deformation is the most likely source of recently observed non-linearities of King plot in  $\text{Yb}^+$ . The results of the combined nuclear and atomic calculations for the effect are consistent with the observations. The contribution of the QFS is about an order of magnitude smaller. The measurements of the non-linearity of the King may be used to study nuclear deformation in nuclei with zero spin where nuclear electric quadrupole moment can not be extracted from atomic spectroscopy. The changes of nuclear charge RMS radii between even-even Yb isotopes extracted from atomic measurements are consistent with nuclear theory.

We are grateful J. Berengut for useful discussion. The work was supported by the Australian Research Council grants No. DP190100974 and DP200100150 and by the US Department of Energy, Office of Science, Office of Nuclear Physics under Grant No. DE-SC0013037

- 
- [1] Ian Counts, Joonseok Hur, Diana P. L. Aude Craik, Honggi Jeon, Calvin Leung, Julian C. Berengut, Amy Geddes, Akio Kawasaki, Wonho Jhe, and Vladan Vuletic, *Phys. Rev. Lett.* **125**, 123002 (2020).
- [2] K. Mikami, M. Tanaka, and Y. Yamamoto, *The European Physical Journal C* **77**, 896 (2017).
- [3] Evaluated Nuclear Structure Data File (ENSDF) located at the website (<http://www.nndc.bnl.gov/ensdf/>) of Brookhaven National Laboratory. ENSDF is based on the publications presented in Nuclear Data Sheets (NDS) which is a standard for evaluated nuclear data.
- [4] S. G. Nilsson and I. Ragnarsson, *Shapes and shells in nuclear structure*, (Cambridge University Press, 1995).
- [5] Z.-H. Zhang, M. Huang, and A. V. Afanasjev, *Phys. Rev. C* **101**, 054303 (2020).
- [6] Saleh O. Allehabi, V. A. Dzuba, V. V. Flambaum, A. V. Afanasjev, and S. E. Agbemava, arXiv:2001.09422 (2020). *Phys. Rev. C*, **102**, 024326 (2020).
- [7] V. A. Dzuba, V. V. Flambaum, P. G. Silvestrov, and O. P. Sushkov, *J. Phys. B: At. Mol. Phys.*, **20**, 1399 (1987).
- [8] V. V. Flambaum and V. A. Dzuba, *Phys. Rev. A* **100**, 032511 (2019).
- [9] E. C. Seltzer, *Phys. Rev.* **188**, 1916 (1969).
- [10] S. A. Blundell, P. E. G. Baird, C. W. P. Palmer, D. N. Stacey, and G. K. Woodgate, *J. Phys. B: At. Mol. Phys.* **20**, 3663 (1987).
- [11] P.-G. Reinhard, W. Nazarewicz, and R.F. Garcia Ruiz, *Phys. Rev. C* **101**, 021301(R) (2020).
- [12] I. Angeli, K. P. Marinova, *Atomic Data Nuclear Data Tables* **99**, 69 (2013).
- [13] D. L. Clark, M. E. Cage, D. A. Lewis, and G. W. Greenlees, *Phys. Rev. A* **20**, 239 (1979).
- [14] W. van Wijngaarden and J. Li, *J. Opt. Soc. Am. B* **11**, 2163 (1994).
- [15] K. Pandey, A. K. Singh, P. V. Kiran Kumar, M. V. Suryanarayana, and V. Natarajan, *Phys. Rev. A* **80**, 022518 (2009).
- [16] Peggy E. Atkinson, Jesse S. Schelfhout, and John J. Mc-

- Ferran, Phys. Rev. A **100**, 042505 (2019).
- [17] V. A. Dzuba, V. V. Flambaum, and M. G. Kozlov, Phys. Rev. A, **54**, 3948 (1996).
- [18] S. Raman, C. W. Nestor and P. Tikkanen, At. Data Nucl. Data Tabl. **78**, 1 (2001).
- [19] S. E. Agbemava, A. V. Afanasjev, D. Ray and P. Ring, Phys. Rev. C **89**, 054320 (2014).
- [20] A. V. Afanasjev and S. E. Agbemava, Phys. Rev. C **93**, 054310 (2016).